Apollo 4 and 6 Radiation Analysis

TIMOTHY T. WHITE* AND ALVA C. HARDY†
NASA Manned Spacecraft Center, Houston, Texas

A primary objective of the unmanned Apollo 4 and 6 missions was to obtain radiation measurements inside an Apollo command module while passing through the most intense portions of the trapped radiation belts. Measurements of the integrated radiation dose behind shields of 0.015 and 0.9 in. of aluminum were made inside the command module on both missions. Dose-rate measurements behind similar shielding were obtained in the Apollo 6 command module during the ascent to apogee. Calculated doses for the missions were within a factor of 2.5 of the measured doses, with better agreement in the calculations for the more thinly shielded sensors. The differences between the calculated and measured doses are, for the most part, attributed to errors in the model environment. The analysis of the Apollo 4 and 6 data indicated that dose calculations for manned lunar missions which pass through the more intense portion of the trapped radiation belt would be reliable and that the expected doses are well below the planning operational dose limits set by NASA.

Introduction

IN recent years, much effort has been directed toward assessing the radiation hazard to manned space flight. It was shown in the Mercury and Gemini programs that high-energy electrons and protons trapped in the magnetic field of the Earth presented no serious problems to low-altitude Earth-orbital flights.[1] However, Apollo missions are planned that will take manned spacecraft through more intense portions of the trapped radiation belts. A primary objective was therefore established to obtain measurements of the radiation dose on the high-altitude Earth-orbital unmanned Apollo 4 and 6 missions. The radiation measurements made on these missions and their comparisons with calculated doses are presented.

Mission Description

The Apollo 4 mission, launched at 7:00 a.m. E.S.T., November 9, 1967, was the first to use a Saturn V launch vehicle and Apollo command and service modules (CSM 017). After approximately two revolutions in a circular parking orbit of 100 naut miles, the S-IVB stage of the Saturn V rocket was used to inject the Apollo command module (CM) into an orbit with an apogee of approximately 9000 naut miles. Twelve minutes after the S-IVB burn, the service propulsion system (SPS) engine was used to raise the apogee to 9767 naut miles. During the 4.5-hr high-altitude orbit, the spacecraft maintained a specific attitude to achieve a thermal gradient across the CM heat shield. Thirty minutes prior to the end of the 8-hr, 41-min Apollo 4 mission, a second SPS burn was made to accelerate the CM to simulate the entry conditions of a lunar-return trajectory.

Apollo 6 used a Saturn V launch vehicle and Apollo CSM 20. Launched on April 4, 1968, the Apollo 6 spacecraft made its first two revolutions in a 100- 200-naut miles elliptical orbit. The SPS engine was then used to inject the CSM into an Earth orbit with an apogee of 12 020 naut miles. Similar to Apollo 4, the spacecraft maintained a specific attitude during the high-altitude portion of the 9-hr, 50-min mission.

One of the primary objectives of both the Apollo 4 and 6 missions was to measure the integrated radiation dose within the CM up to an altitude of at least 2000 naut miles. Another objective of the Apollo 6 mission was to measure the radiation dose rate within the Apollo CM. These measurements were to be used to verify the capability of analytically calculating the radiation dose for a specific spacecraft and trajectory. These objectives were successfully met on both missions.

Radiation Instrumentation

Instruments developed at the Manned Spacecraft Center (MSC) were used to make radiation measurements on the Apollo 4 and 6 missions. An integrating radiation dosimeter (IRD) was flown on each of these missions with the addition of the Van Allen belt dosimeter (VABD) on Apollo 6. These instruments provided the first radiation measurements inside a vehicle to be used in manned space flights, which passed through the most intense portion of the inner radiation belt.

The IRD was designed to provide a measurement of the integrated radiation dose for the entire mission. This instrument measured the integrated dose behind two different shield thicknesses (0.015 and 0.9 in of aluminum), which are approximately equivalent to the 0.07-mm and 5-cm depth in tissue used in the establishment of the NASA skin and depth dose limits for manned missions. The IRD was located near the center of the CM and was attached to the top of the battery support box which was located at a position normally occupied by the center crew couch.

The IRD consisted of two personal radiation dosimeters (PRD) and an aluminum mounting structure. The PRD is being used by the crew of manned Apollo missions to monitor the amount of radiation dose each individual accumulates during a mission. The PRD consists of a 7-cc tissue-equivalent ion chamber, the necessary electronics, and the self-contained battery power supply. A five-digit electromechanical register with a range of 0 to 1000 rad, in 0.01-rad/pulse increments, is used for the integrated dose read-out.[2] The aluminum mounting structure was built for the Apollo 4 and 6 missions to accommodate two PRDs in such a way that the ion chamber-end of one PRD was unshielded and the corresponding end of the other PRD was covered by 0.9 in. of aluminum.

The VABD was designed to measure the radiation dose rates inside the CM on all manned Apollo missions which ex-

Presented as Paper 69-17 at the AIAA 7th Aerospace Sciences Meeting, New York, January 20–22, 1969; submitted February 5, 1969; revision received March 26, 1970.

* Aerospace Technologist, Lunar Missions Office.
† Aerospace Technologist, Space Physics Division.

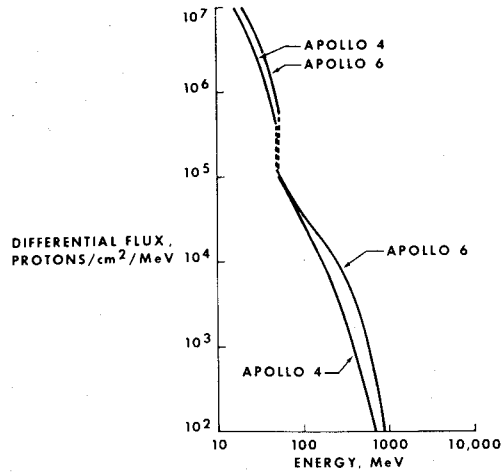

Fig. 1 Apollo 4 and 6 proton differential energy spectra.

tend beyond the nominal 100- to 200-naut miles orbit. The VABD was located in the Apollo 6 CM on the girth shelf underneath the right-hand window. The dose-rate information was telemetered during the flight to the Mission Control Center, where it was recorded and displayed at the space environment console. The VABD measurements were not obtained during the descending portion of the Apollo 6 high-apogee ellipse because of electrical noise on the output signal of the dosimeter caused by a cross-coupling effect with another telemetry signal.

The sensors of the VABD are two 10-cc tissue-equivalent ionization chambers and have shield thicknesses similar to those of the IRD. The unshielded ion chamber on top of the VABD has a wall thickness of 0.04 in. of aluminum. The second ion chamber is shielded by a 0.9-in.-thick hemispherical aluminum shield. The analog output of the instrument, 0 to 5 v d.c., corresponds to dose rates from either 0.01 to 10 rad/hr or 1.0 to 1000 rad/hr. The range of each ion chamber is automatically selected and indicated on a third analog channel.[2]

Measurements and Analysis

A radiation analysis of the Apollo 4 and 6 flights has been made by using the MSC Orbital Dose Code (MODC) and tracking data obtained from the Manned Space Flight Network. The MODC selected positions on the trajectory at 15-sec intervals and determined the corresponding geomagnetic coordinates (B,L) by using the McIlwain field-fit code[3] and Jensen and Cain coefficients.[4] The electron and proton fluxes and energy spectra are then determined from the Vette

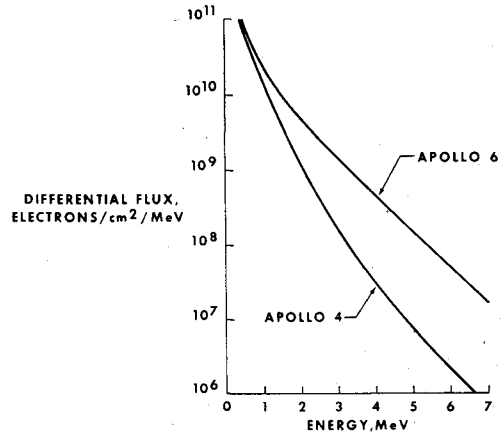

Fig. 2 Apollo 4 and 6 electron differential energy spectra.

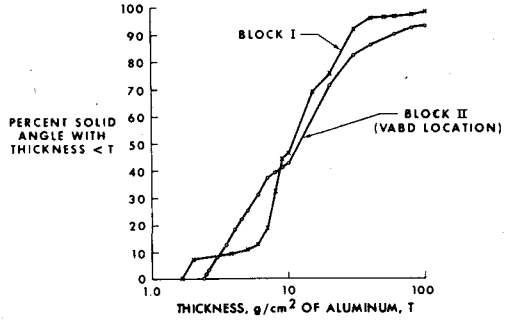

Fig. 3 Apollo command and service module shielding distribution.

AP1-4 proton environment[5] and AE2 electron environment.[6] The electron fluxes were decayed by using the mean-life decay factor for various L shells of Bostrom and Williams.[7] The MODC cumulative proton and electron differential energy spectra for the Apollo 4 and 6 missions are shown in Figs. 1 and 2. The MODC, using data from MSC dose programs,[8] attenuated the particle environment through the analytical spacecraft shielding description to a specified dose point and computed the resultant energy deposition or dose.

The spacecraft analytical-shielding geometry used in the IRD dose calculations was the Apollo Block I (BK-I) CM shielding description. A shielding profile for this geometry is shown in Fig. 3. Only one dose point was available for this description which, fortunately, was near the IRD location in the Apollo 4 spacecraft. The difference between calculated and measured doses due to the different dose point location was expected to be small since the spacecraft is reasonably symmetric about this area. The IRD geometry was represented by adding spherical shields of 0.103 g/cm² (0.015 in.) and 6.17 g/cm² (0.9 in.) of aluminum to the BK-I shielding description. The measured and calculated IRD doses for the Apollo 4 and 6 missions are shown in Table 1. Most of the calculated IRD doses were caused by inner-belt protons with the sum of the primary electron and bremsstrahlung doses contributing less than 20% to the total doses.

Table 1 shows that the Apollo 6 measured doses were higher than the Apollo 4 measured doses by approximately a factor of 2. Although both the Apollo 4 and 6 trajectories followed roughly the same path through the inner belt, Apollo 6 spent more time in the region of highest proton intensity (as shown in Fig. 4) and, therefore, should have encountered

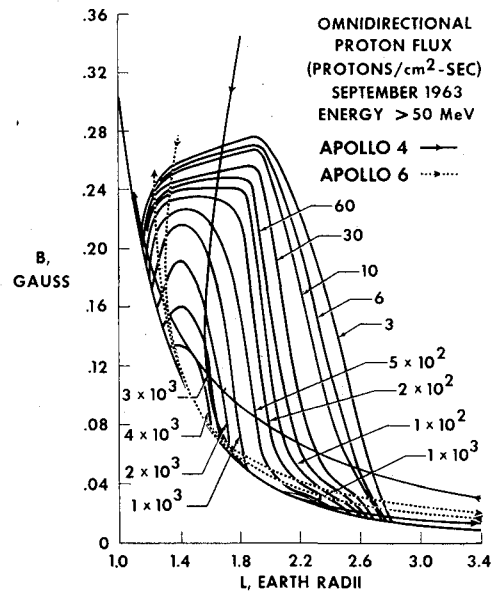

Fig. 4 B, L trace of the Apollo 4 and 6 trajectories.

Table 1 Measured and calculated Apollo 4 and 6 IRD doses

	Dosimeter shield thickness, g/cm² of aluminum	Dose, rad	
		Measured	Calculated
Apollo 4	0.1	0.59	0.71
	6.17	0.38	0.2
Apollo 6	0.1	1.31	1.27
	6.17	0.9	0.36

more radiation. It is also noted in Table 1 that the calculated doses for the unshielded IRD sensors are very close to the measured doses, which are 20% higher for Apollo 4 and 3% lower for Apollo 6. The calculated doses for the shielded sensors are lower than the measured doses by approximately a factor of 2.

The differences between the calculated and measured doses for the IRD shielded sensor suggest that the model proton environment may be inaccurate at high energies. Fig. 5, which gives the percentages of the total Apollo 6 IRD doses resulting from protons having incident energies greater than E, shows that the dose measured by the shielded sensor was caused by protons whose incident energies were greater than 90 Mev. This indicates that the high-energy proton fluxes given in the Vette AP3 proton environment are too low. This premise is supported by data from the Flight Experiment Shielding Satellite (FESS) experiment in 1965[9] and measurements made on OV3-4 in 1966,[10] which show that the Vette high-energy proton environment is, in general, too low and often by as much as a factor of 4 or 5.

The analytical BK-I shielding description could not be used in the VABD calculations since the dose point in the BK-I description located at the center of the spacecraft was greatly different from the location of the VABD near the wall of the Apollo 6 spacecraft. An analytical description of the Block II (BK-II) CM obtained from North American Rockwell was used to generate the shielding about the VABD location (Fig. 3). The geometries for the VABD sensors were represented by adding spherical shells of 0.227 g/cm² and 6.34 g/cm² of aluminum, respectively. The major difference between the BK-I and BK-II descriptions was the thicker heat shield used in the BK-II description. The effect of using the BK-II description in the VABD dose calculations was estimated by calculating VABD doses at the center of both vehicles using the cumulative Apollo 6 proton energy spectrum. The VABD calculated doses for the BK-II description were lower than those for the BK-I description by approximately 35% for the unshielded sensor and 13% for the shielded sensor. The calculated dose rates for the VABD using the BK-II geometry were changed accordingly so they could be compared with the measurements in the BK-I vehicle.

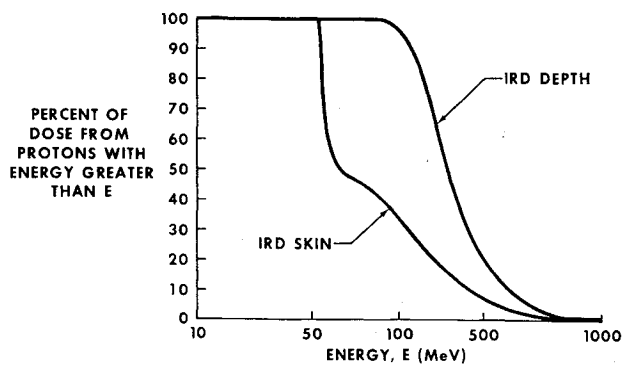

Fig. 5 Percent of dose from protons with energy greater than E compared with E (Apollo 6 spectra).

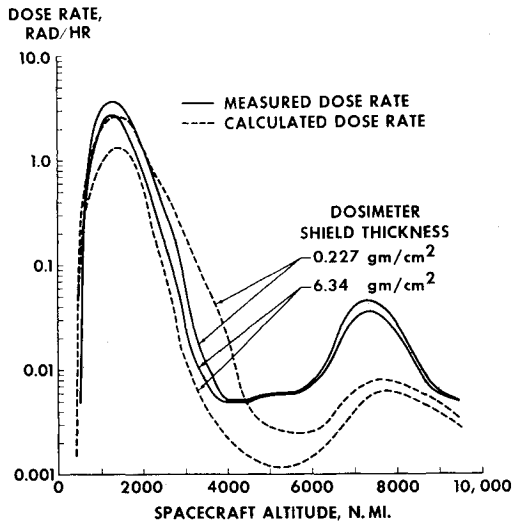

Fig. 6 Apollo 6 measured and calculated dose rates compared with altitude.

The measured and calculated VABD dose rates encountered during the ascending portion of the Apollo 6 high-altitude orbit are shown in Fig. 6. Peak dose rates of 3.6 and 2.6 rad/hr for the unshielded and shielded sensors, respectively, resulted from high-energy protons encountered as the spacecraft passed through the most intense portion of the inner radiation belt (1300 naut miles). Dose rates of 0.045 and 0.036 rad/hr were measured as the spacecraft passed through the outer radiation belt (7600 naut miles). These dose rates were due to bremsstrahlung photons produced by the interaction of the outer belt electrons with the spacecraft shielding. The Apollo 6 dose-rate measurements indicate that extended operation of a manned Apollo CM at altitudes between 800 and 2400 naut miles would be severly limited because of dose rates in excess of 1 rad/hr. Astronaut activity in more thinly shielded vehicles than the CM, such as the lunar module, or in space suits would most likely be prohibited at these altitudes.

The calculated inner-belt dose rates for the unshielded VABD sensor (Fig. 6) compare well with the measurements below an altitude of 2200 naut miles, but are too high above this altitude. The calculated inner-belt dose rates for the shielded VABD sensor are, in general, much lower than the measurements. These data are similar to the results of the IRD analysis; e.g., poorer agreement is obtained for the shielded sensor with the calculated dose rates being lower than the measurements.

The calculated VABD dose rates for the passage through the outer radiation belt (Fig. 6) are lower than the measurements by a factor of 6, indicating that the electron flux used in the calculations was low by a similar amount. The difference between the outer-belt electron environment indicated by the Apollo 6 measurements in 1968 and the electron environment during 1962 and 1964 used in the calculations might be explained by short-term fluctuations in the outer-belt electron intensity. However, it may be evidence of an enhancement in the outer-belt electron intensity caused by the increased solar activity during the maximum of the solar cycle.

Concluding Remarks

Dose calculations for the Apollo 4 and 6 missions are within a factor of 2.5 of the integrating radiation dosimeter measurements. These differences are well within the state of the art for such complex computations. Although the need for a more accurate model of the trapped radiation environment is indicated, the results of the radiation analysis lend a great deal of confidence to the use of analytical computations for

mission planning. These missions show that there will be no biological hazard associated with passage through the trapped radiation belts during the translunar and trans-Earth phase of Apollo lunar missions, providing that there are no further high-altitude nuclear tests and that astronaut activity is confined to the command module during belt passage.

The Apollo 4 and 6 radiation analysis shows that a certain degree of proficiency has been obtained in estimating the potential radiation encountered by spacecraft passing through the trapped radiation belts. However, since the possibility of a radical change in the trapped radiation environment exists, manned space vehicles will be supplied with sufficient radiation-monitoring instrumentation to provide real-time evaluation of this environment.

References

[1] Higgins, P. W., Lill, J. C., and White, T. T., *Radiation Environment at High Orbital Altitudes*, NASA SP-138, 1967, pp. 149–157.

[2] Richmond, R. G. et al., *Radiation Dosimetry for Manned Space Flight*, NASA SP-169, 1968, pp. 555–580.

[3] McIlwain, C. E., "Coordinates for Mapping the Distribution of Magnetically Trapped Particles," *Journal of Geophysical Research*, Vol. 66, Nov. 1961, pp. 3681–3691.

[4] Jensen, D. C. and Cain, J. C., "An Interim Geomagnetic Field," *Journal of Geophysical Research*, Vol. 67, Aug. 1962, pp. 3568–3569.

[5] Vette, J. I., *Models of the Trapped Radiation Environment Vol. I: Inner Zone Protons and Electrons*, NASA SP-3024, 1966.

[6] Vette, J. I., Lucero, A. B., and Wright, J. A., *Models of the Trapped Radiation Environment, Vol. II: Inner and Outer Zone Electrons*, NASA SP-3024, 1966.

[7] Bostrom, C. O. and Williams, D. J., "Time Decay of the Artificial Radiation Belt," *Journal of Geophysical Research*, Vol. 70, Jan. 1965, pp. 240–242.

[8] Hardy, A. C., Lopez, M. D., and White, T. T., *A Parametric Technique of Computing Primary Electron Dose*, edited by A. Reetz and K. O'Brien, NASA SP-169, 1968, pp. 391–401.

[9] Chapman, M. C. et al., "Phase I Analysis of Data Returned by the FESS Experiment from the OV 1-2 Spacecraft," Contract AF 29(601)-7038, AFWL-TR-66-94, March 1967, U.S. Air Force.

[10] Thede, A. L. and Radke, G. E., *A Correlation of Dosimetric Measurements with Charged Particle Environment of the Inner Van Allen Belt*, edited by A. Reetz and K. O'Brien, NASA SP-169, 1968, pp. 75–92.

JULY 1970 J. SPACECRAFT VOL. 7, NO. 7

Model for the Prediction of Closed Compartment Fire Propagation

M. Bello* and A. L. Johnson†
The Aerospace Corporation, El Segundo, Calif.

A one-dimensional (radial) mathematical model of a closed compartment fire is developed to 1) analyze the effects of various combustion parameters and 2) predict the composition, pressure, and temperature histories of the atmosphere during a fire. A semiempirical expression is formulated to relate the average linear burning rate of the combustile materials and the flame propagation which includes the effects of convective velocity, gravity, total pressure. and oxygen partial pressure. A computer program is used to solve the equations resulting from the heat, mass, and combustion equations. The results of this analysis provide a macroscopic overview of a fire in a closed compartment.

Nomenclature

A = surface area of compartment, in.^{2}
a = surface area of a sphere ($4\pi r^2$), in.^{2}
C_g = thermal capacitance of gaseous atmosphere, Btu/°R
C_m = thermal capacitance of compartment mass, Btu/°R
c_p = specific heat at constant pressure, Btu/lb-°R
g = magnitude of gravitational field, ft/sec^2
Gr = Grashof number
h = film coefficient, Btu/in.^{2}-sec-°R
Δh_c = heat of combustion of burning material, Btu/lb
k = thermal conductivity of gas, Btu/in.-°R-sec
L = characteristic length, in.
l = linear sample burn distance, in.
Nu = Nusselt number
Pr = Prandtl number
P_T = total atmospheric pressure, psia
$\dot{q}_k$ = gas conduction heat rate, Btu/sec
$\dot{q}_c$ = convective heat rate, Btu/sec
$\dot{q}_v$ = heat of evaporization or condensation, Btu/sec
$\dot{q}_r$ = radiation heat rate, Btu/sec
$\dot{q}_T$ = total heat rate from the combustion region, Btu/sec
$\dot{q}_\beta$ = burning rate heat rate, Btu/sec; $\dot{q}_{\beta 1}$, to gas; $\dot{q}_{\beta 2}$, to mass
R_k = conduction resistance, sec-°R/Btu
R_c = convection resistance, sec-°R/Btu
R_r = radiation resistance, sec-°R/Btu
r = radius of spherical flame front, in.
r_i = radius of initial flame front, in.
r_o = radius of spherical model, in.
r_s = equivalent radius of sample, in.
Re = Reynolds number
T_f = flame temperature, °F
T_g = bulk gas temperature, °F
T_m = bulk equipment mass temperature, °F
t = time (independent variable), sec
V = volume of material, in.^{3}
v = velocity of circulating gas, in./sec
W = mass, lb
x = experimental exponents
Y = mole fraction
y = experimental exponents
α = area burning rate, in.^{2}/sec
β = convective linear burning rate, in./sec
β_s = experimental linear burning rate of a particular sample, in./sec

Presented as Paper 69-618 at the AIAA 4th Thermophysics Conference, San Francisco, Calif., June 16–18, 1969; submitted December 4, 1969, revision received February 24, 1970.

* Member of the Technical Staff, Thermal Systems and Cryogenics Section, Applied Mechanics Division.

† Section Manager, Thermal Systems and Cryogenics Section, Applied Mechanics Division.